scientific reports

Check for updates

OPEN

Phosphorous modified cocopeat biochar as a low cost, efficient and stable adsorbent for the removal of Cu(II) and Ni(II) from aqueous and real systems

Sadamanti Sireesha & I. Sreedhar✉

Biochar is widely acknowledged as an environmentally efficient adsorbent for removing heavy metals from wastewater. However, its practical application is often limited by insufficient adsorption capacity. This limitation primarily arises from low surface area, suboptimal selection and utilization of chemical activating agents, and inadequate development of surface functional groups, leading to reduced stability. To address these challenges, the present study focuses on the synthesis and application of phosphoric acid-activated non-edible coco peat biochar (PMCB) for the efficient and stable removal of Cu^{2+} and Ni^{2+} from both aqueous solutions and real wastewater systems. Thus, this study focuses on the synthesis and application of phosphoric acid-impregnated non edible coco peat biochar (PMCB) for efficient and stable removal of Cu^{2+} and Ni^{2+} from both aqueous and real systems. The PMCB was prepared at combined optimal conditions (Pyrolysis temperature and H_3PO_4 impregnation ratio), which improved its physicochemical properties compared to that of pristine biochar. The PMCB exhibited superior adsorption capacities of 566.6 mg/g and 551.7 mg/g for Cu^{2+} and Ni^{2+} in batch tests and 794.5 mg/g and 691.4 mg/g in column studies. The adsorption data by PMCB were well fitted by the Langmuir isothermal and pseudo-second-order kinetic models, indicating monolayer chemical adsorption controlled the adsorption process. Characterisation using XPS and FTIR confirmed the presence of $-PO_3$ and $-PO_4$ functional groups in the modified biochar. These functional groups enhance metal adsorption through precipitation, physicochemical adsorption, surface complexation, ion exchange, and electrostatic interactions. PMCB demonstrated 99% removal efficiency for metals and pollutants in single-component and real-world systems. Stability tests showed PMCB's reusability for up to 20 cycles with a 96.0% desorption rate. Additionally, the spent biochar proved effective as a bio-fertilizer. Cost analysis confirmed PMCB to be economically viable at 1.56 USD/kg (130.7 INR/kg), making it a cost-effective, sustainable, and low-energy solution for industrial heavy metal removal and wastewater treatment.

Keywords Real effluent treatment, Biochar reusability, Column adsorption, Hierarchical optimization, Biofertilizer

Water is crucial for the survival of all living beings. However, industries such as metal plating, battery manufacturing, metallurgy, mining and fertilizer manufacturing are among the primary sources of water contamination with heavy metals[1,2]. Due to their toxic, non-biodegradable, mutagenic, and carcinogenic properties, it is essential to treat heavy metals correctly before their release into the environment[3–5]. Various methods have been employed to remove heavy metals from water, including precipitation, coagulation method[6], ion exchange, membrane separation, and adsorption[7]. Out of all these methods, adsorption has been widely employed as a way of removing heavy metal ions. Its economic viability, parameters, and minimal sludge volume are shown to be some of the significant advantages[8].

Department of Chemical Engineering, BITS Pilani Hyderabad Campus, Hyderabad 500078, India. ✉email: isreedhar@hyderabad.bits-pilani.ac.in

Biomass based adsorbents offer promising alternatives to address various environmental and financial challenges which are inherent in other treatment methods. Factors such as metal types, functional groups, surface area, and other adsorbent characteristics are pivotal in the binding of metals with biochar[9,10]. Despite persistent challenges such as production complexity and the need for expensive reagents and equipment, agricultural and industrial wastes like coco peat, rice husk, neem bark, slag, coconut shell, and peanut husk are commonly utilized for adsorption processes[11]. The Food and Agriculture Organization (FAO) highlights the significant production of coconut residue in tropical regions where coconut trees are prevalent. Leading countries in coconut cultivation, such as Indonesia (17.1 million tonnes), India (14.7 million tonnes), Sri Lanka (2.5 million tonnes), Brazil (2.33 million tonnes), Vietnam (1.68 million tonnes), along with various African nations, generate substantial amounts of coconut residue[12]. Therefore, in this investigation, coco peat is utilized as the primary material for developing adsorbents to adsorb Cu^{2+} and Ni^{2+} from both single and real effluent systems.

Various studies have been conducted on functional groups, surface area, surface charge, and binding capacity of biochar are enhanced using various reagents, such as hydrochloric acid, potassium hydroxide, sodium hydroxide, and phosphoric acid[4,13–15]. Among the mentioned acids, phosphoric acid can be considered environmentally friendly. Phosphoric acid acts as a dehydrating agent, removing water molecules from the biochar structure. The dehydration process enhances the surface area of biochar, allowing for greater adsorption capacity of heavy metal ions. Additionally, this treatment increases the thermal stability and chemical resistance of biochar, making it more durable in harsh environments[16–19]. However, few studies have explored the use of phosphoric acid-treated (PAT) biochar, derived from different feedstocks, for effective metal removal[20–23]. Previous studies suggest that PAT biochar holds promise as an economical candidate for wastewater treatment. Despite this, there is limited investigation into the combined optimal pyrolysis temperature and H_3PO_4 concentration for PAT biochar production. Most of the research has primarily been on batch tests to evaluate PAT candidates' uptake capacity and behaviour for removing Cu^{2+} and Ni^{2+}. Additionally, the ability of these adsorbents to remove multiple contaminants from actual effluent is not well discussed. PAT adsorbents tend to lose their reductive properties after initial use, making the regeneration process difficult. Most of the previous studies have focused on their single-use application for metal removal but have not focused much on the lifecycle of the adsorbent and reusability[20,24–26]. The motivation behind this study is to fill above mentioned research gaps by providing comprehensive solutions. The primary focus of this study is on real-world systems collected from the battery industry, which contain high concentrations of copper, nickel, and other pollutants. Additionally, the study aims to find effective ways to manage spent adsorbent to minimize secondary pollution.

This study addresses existing research gaps by offering comprehensive solutions for removing heavy metals specifically those from the battery industry, which often contain high concentrations of copper, nickel, and other contaminants. It focuses on optimizing PMCB's physicochemical properties through ideal H_3PO_4 concentration and pyrolysis temperature, followed by a three-level process optimization: (i) optimizing adsorbent properties, (ii) applying RSM to refine process parameters and maximize efficiency, and (iii) optimizing pH (surface charge) and temperature (thermodynamic analysis) for ideal removal performance. This multi-level strategy ensured maximum adsorption efficiency. The competitive behaviour of Cu^{2+} and Ni^{2+} is analysed in multisystem and real-world scenarios. The study also explores strategies for managing spent adsorbent to minimize secondary pollution and confirms the economic viability of the biochar production, highlighting its potential for effective environmental pollution control.

Materials and methods

Synthesis of PMCB

The purity of chemicals and raw materials used for biochar preparation is demonstrated in Sec.S1. CP (cocopeat) was thoroughly washed with tap water to remove impurities and then sun-dried for seven days. The resulting material was sieved to achieve a particle size of 300 µm which was named coco peat adsorbent (CB). In Sec. S2 and Table.S1-S2, a detailed analysis of the first level optimization process of H_3PO_4 concentration and its corresponding pyrolysis temperature is presented, addressing a critical research gap. In brief, the dried CB was treated with various concentrations of H_3PO_4 solution (CB to acid ratio of 1:5) and left for 24 h at ambient temperature for impregnation. Then, the sample was packed into earthen pots, sealed to minimize oxygen exposure, and gradually heated (heat rate of 278 K/min) in a muffle furnace up to different temperatures for 2 h. After cooling, the sample was washed until it reached a neutral pH. This method produces up to 65.2% biochar, with the synthesis protocol depicted schematically in Fig. 1. Various analytical methods were employed to characterize the physical and chemical properties of PMCB before and after adsorption. A detailed explanation of each instrument has been discussed in Sec.S3.

Adsorption experiments in batch mode

Adsorption experiments in batch processes are essential for understanding the interaction between heavy metals and PMCB under controlled conditions. The detailed explanation can be seen in Sec.S4. These experiments help determine the adsorption capacity, kinetics, and equilibrium characteristics of the PMCB.

Adsorption experiments in a column mode

Column experiments are essential for understanding the dynamics of adsorption processes under realistic conditions, aiding in the efficient removal of contaminants. The detailed column fabrication is explained in Sec.S5 and Fig.S1. The economic feasibility and the ability to reduce secondary pollution of adsorbents are significantly determined by their reusability[27]. Sec.S6 provides a detail procedure for regeneration studies.

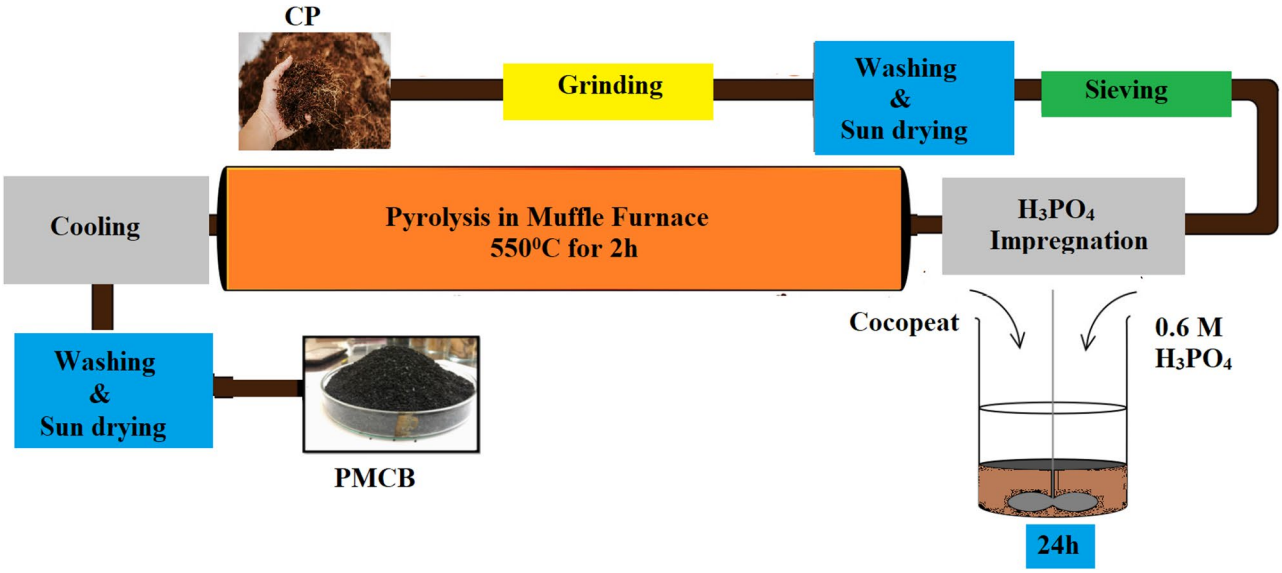

Fig. 1. Schematic representation of PMCB preparation method for Cu^{2+} and Ni^{2+} removal.

Results and discussion

Three level process optimization in batch mode

In batch mode, hierarchical optimization is employed to refine parameters for enhanced heavy metal removal. The first level focuses on optimizing H_3PO_4 concentration and pyrolysis temperature to improve biochar properties. The second level applies Response Surface Methodology (RSM) to statistically refine conditions by analyzing parameter interactions. Finally, the third level fine-tunes operational factors like pH and temperature to maximize adsorption efficiency. This structured, stepwise approach ensures systematic optimization, addressing key research gaps and enhancing the practical applicability of the developed adsorbent.

Second-level process optimization via RSM

Efficient utilization of the adsorbent involves maximizing adsorption capacity while minimizing factors like contact time and PMCB dosage to achieve maximum metal removal while minimizing costs and energy consumption[28]. To carry out this optimization, a Central composite design (CCD) based approach integrated with RSM was employed. Table S3 outlines the range of values considered for the independent variables, while Table 1 shows the designed experiments generated based on input factors (concentration, contact time and dosage) and out response (adsorption capacity) by using the CCD approach for copper and nickel.

The adsorption capacity of PMCB adsorbent is given by Eqs. 1 and 2 respectively. Both equations were derived through regression analysis using Response Surface Methodology (RSM), relating the independent variables such as concentration (A), contact time (B), and adsorbent dosage (C) to the adsorption capacity. The equations were fitted to the experimental data (Table 1) to predict responses and identify optimal process conditions.

$$\begin{aligned}\textbf{Response 1}\ \left(\mathbf{R_{Cu}}^{2+}, \mathbf{mg/g}\right) &= 13.89 + 4.33^{*}\mathrm{A} + 0.1098^{*}\mathrm{B} - 4.29^{*}\mathrm{C} - 0.0247^{*}\mathrm{AB} \\ &\quad - 1.31^{*}\mathrm{AC} - 0.1129^{*}\mathrm{BC} - 0.9304^{*}\mathrm{A}^{2} - 0.1494^{*}\mathrm{B}^{2} + 1.27^{*}\mathrm{C}^{2}\end{aligned} \quad (1)$$

$$\begin{aligned}\textbf{Response 2}\ \left(\mathbf{R_{Cu}}^{2+}, \mathbf{mg/g}\right) &= 13.62 + 4.46^{*}\mathrm{A} + 0.1301^{*}\mathrm{B} - 4.30^{*}\mathrm{C} - 0.0503^{*}\mathrm{AB} \\ &\quad - 1.24^{*}\mathrm{AC} - 0.0868^{*}\mathrm{BC} - 0.9894^{*}\mathrm{A}^{2} - 0.1646^{*}\mathrm{B}^{2} + 1.18^{*}\mathrm{C}^{2}\end{aligned} \quad (2)$$

Analysis of Variance (ANOVA) was performed to assess the significance of the obtained quadratic model. The p-value is less than 0.0001, indicating that the model is highly significant. Additionally, the adjusted R^2 and predicted R^2 values were both similar and close to one for Cu^{2+} and Ni^{2+} (the adjusted R^2 values were 0.97 and 0.96, respectively, while the predicted R^2 values were 0.98 and 0.97 for both metals. This underscores the models' suitability for representing the adsorption capacity for both metals. In Fig. 2a, it was observed that when the contact time increased, the adsorption capacity also increased. This can be attributed to the increased probability for metal ions to reach the pores of the adsorbent over time. However, once the adsorbent was saturated, the adsorption capacity reached a plateau and remained constant despite further increases in contact time. In Fig. 2a1, the adsorption capacity initially rose with PMCB dosage and the metal ions' initial concentration. However, beyond a certain point, the capacity started to decline. This decline is likely due to the saturation of the surface of PMCB with Cu^{2+} ions. Moreover, at higher initial concentrations, interactions between particles, such as aggregation, reduce the adsorption capacity. Figure 2a2 also showed a higher adsorption capacity with increasing contact time and PMCB dosage as a longer contact time allows for more utilization of available adsorption sites on the adsorbent. The Fig. 2a3 graph (Predicted vs. Actual) showed RSM model accuracy, where closer

Run	Factor 1 A: Concentration (mg/L)	Factor 2 B: Contact Time (h)	Factor 3 C: Dosage (g/L)	Response 1 Adsorption capacity Cu^{2+} (mg/g)	Response 2 Adsorption capacity Ni^{2+} (mg/g)
1	100	4	2	50	40
2	350	1.5	2	173.4	163.4
3	350	4	0.6	583.0	563.04
4	225	2.8	1.3	190	180
5	225	2.8	1.3	197.7	187.7
6	100	1.5	0.6	153.8	143.8
7	100	1.5	2	50	40
8	100	4	0.6	166.7	156.2
9	225	2.8	1.3	191.6	181.6
10	225	2.8	1.3	195.8	185.8
11	350	4	2	172.4	162.4
12	350	1.5	0.6	566.1	556.1
13	435.2	2.8	1.3	332.3	329.3
14	225	2.8	1.3	190	189
15	225	2.8	1.3	192.5	190.5
16	225	4.8	1.3	180.0	178.2
17	14.8	2.8	1.3	14.5	10.2
18	225	2.8	0.12	620	590
19	225	2.8	2.5	91.6	87.2
20	225	0.64	1.3	169.4	160.2

Table 1. CCD analysis and design experiments for Cu^{2+} and Ni^{2+} removal using PMCB.

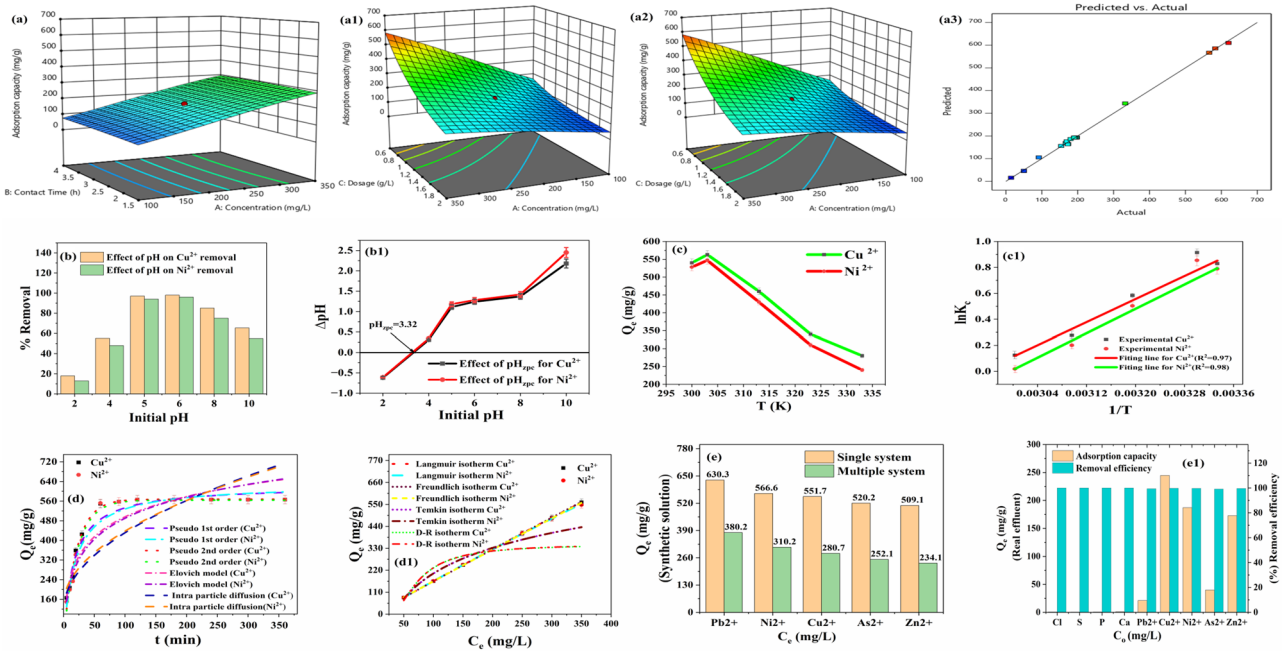

Fig. 2. Multi-parameter optimization and modelling for Cu^{2+} and Ni^{2+} adsorption on PMCB: **(a-a3)** Effects of contact time, concentration, and dosage **(b-b1)** Influence of pH and pH_pzc on removal efficiency **(c-c1)** Temperature impact (300–333 K) **(d-d1)** Kinetic and isotherm models **(e-e1)** Impact of coexisting ions in different system.

alignment of data points to the diagonal line signifies high predictive reliability for adsorption capacity. Similar trends as stated above were observed for Ni^{2+}. The optimal values for concentration, PMCB dosage, and contact time were determined to be 350 mg/L, 0.6 g/L, and 1.5 h respectively. The importance level for minimizing contact time and dosage was set at level 4, whereas the importance level for maximizing adsorption capacity

was set at level 5. At these optimal conditions, the adsorption capacity predicted by the model (566.7 mg/g for Cu^{2+} and 551.7 mg/g for Ni^{2+}) closely aligned with the experimental values, showing a minor deviation of 1.05% (564.85 mg/g for Cu^{2+} and 551.3 mg/g for Ni^{2+}). These results demonstrate significant improvement over recently reported findings[29,30].

Third-level process optimization

Optimization of pH The adsorption process depends on many factors, such as the acidity of the solution and the surface charge of the adsorbent[31,32]. To investigate the effect of pH on the adsorption of Cu^{2+} and Ni^{2+} onto PMCB, a pH range from 2 to 10 was studied, with pH levels adjusted using 0.1 M HCl and 0.1 M NaOH as shown in Fig. 2b. As pH increased from 2 to 6 we saw an increase in adsorption percentages for both Cu^{2+} and Ni^{2+}, peaking at pH 6. At low pH values (2–4), the biochar surface was highly protonated and positively charged, leading to significant competition from H^+ ions for adsorption sites, thereby reducing the efficiency of metal ion removal[33]. In the moderately acidic to neutral range (pH 5), the biochar began to deprotonate, reducing the positive charge and making more phosphate groups (PO_4^{3-}) available for binding Cu^{2+} and Ni^{2+}. This resulted in improved adsorption efficiency as the competition from H^+ ions decreased. At pH 6, phosphate groups on the biochar surface predominantly exist as $H_2PO_4^-$ and HPO_4^{2-} ions. These species facilitate the formation of surface complexes with Cu^{2+} and Ni^{2+} ions, where the metal ions directly coordinate with the oxygen atoms of phosphate groups (e.g., M–O–PO_3H^-, M = Cu or Ni), enhancing metal adsorption[34–36]. When the pH was neutral to slightly alkaline (pH 7), the biochar surface became further deprotonated, becoming neutral or slightly negatively charged, enhancing electrostatic attraction to the positively charged metal ions and their complexes, making this range optimal for adsorption. However, at higher pH values (8–10), the biochar surface became predominantly negatively charged, and Cu^{2+} and Ni^{2+} tended to form insoluble hydroxide precipitates such as $Cu_3(PO_4)_2$ and $Ni_3(PO_4)_2$. These phosphate precipitates contributed to higher adsorption capacities due to their solid nature in aqueous solutions, as confirmed by XPS analysis. The results showed significant improvement in adsorption capacities when compared to the reported studies[13,37–39]. However, the efficiency of metal ion removal declined as more metal precipitated out of the solution rather than being adsorbed onto the biochar surface. These mechanisms highlighted the optimal conditions for effective biochar-based adsorption processes, typically found in the neutral to slightly alkaline pH range, around pH 6, for both metals in the experiment. Point zero charge (pH_{zpc}) characterization evaluated PMCB's surface charge at different pH levels. Figure 2b1 shows that PMCB exhibits a point of zero charge (pH_{zpc}) at pH 3.32, with optimal adsorption occurring at pH 6 for both Cu^{2+} and Ni^{2+}. This indicates that at pH 6, the PMCB surface is negatively charged, enhancing the adsorption of these positively charged metal ions. Therefore, it is recommended that adsorption of Cu^{2+} and Ni^{2+} effluents be carried out at pH 6 for industrial processes.

Optimization of temperature Optimization of temperature involves maximizing efficiency while minimizing energy consumption and environmental impact[40]. The experimental data obtained revealed that within the temperature range of 300 to 333 K, temperature influenced the metal adsorption. As depicted in Fig. 2c, the adsorption of both metal ions is most pronounced at around 303 K and gradually declines with further increase in temperature. The highest Cu^{2+} and Ni^{2+} removal was achieved at 303 K, with adsorption capacities of 563 mg/g and 543 mg/g respectively. The reduced adsorption at higher temperatures could be attributed to the diminished electrostatic forces between the metal ions and PMC[41]. The thermodynamic properties were calculated using equations from the literature[42,43] to study the feasibility of the process. The data in Fig. 2c1 and Table S4 indicated favourable thermodynamics for both metals' sorption on PMCB across different temperatures. The equilibrium constant (K_c) increases for both metals, indicating heightened affinity. The ΔH^0 and ΔS^0 values of −16.6 kJmol^{-1} and − 54.3 Jmol^{-1}.K^{-1} respectively, for Cu^{2+} and − 18.02 kJmol^{-1} and − 58.4 Jmol^{-1}.K^{-1}, respectively, for Ni^{2+} were obtained with the help of slope and intercept of the graph of the Vant't Hoff equation. The negative ΔH^0 for both metals signifies an exothermic reaction, suggesting the involvement of physisorption process[44,45]. The negative ΔS^0 for both metals signifies reduced randomness at the interface between PMCB and the solution during sorption[43,46]. The negative ΔG^0 values indicate that the adsorption of Cu^{2+} and Ni^{2+} onto PMCB is thermodynamically spontaneous, implying a natural tendency of the metal ions to bind to the adsorbent surface without external energy input. A strong correlation for both metals ($R^2_{Cu^{2+}} = 0.97$ and $R^2_{Ni^{2+}} = 0.98$) between experimental and model data indicates reliable predictions.

Kinetic and isotherm studies

The study used both linear (Fig.S2 and S3) and nonlinear (Fig. 2 (d-d1)) kinetic and isotherm models to analyze the data. Recent literature indicates that nonlinear fitting is rarely used in isotherm-kinetic studies because of challenges in data collection and plotting, which hinder better convergence[2,47,48]. Consequently, linear models were specifically employed to explain and fit the experimental data. Linearized models for kinetic, isotherm, and thermodynamic studies are popular due to their simplicity, enabling a more accurate assessment of fitting parameters. Pseudo-first, second order, elovich and multistage stage fitting of intra-practical diffusion models were used to fit the collected data and to identify the best model for the adsorption of both metals on PMCB[49,50]. The calculated kinetic parameters are presented in Table S5, and the graphical analysis of these kinetic models is shown in Fig. S2. The pseudo-first-order model (Fig. S2a) indicates physisorption interactions between PMCB and metals, with R^2 values ranging from 0.96 to 0.97 for both metals. In contrast, the pseudo-second-order model (Fig. S2b), which assumes chemisorption, demonstrated that the calculated q_e values closely match the experimental q_e values (see Table S5), with R^2 values between 0.98 and 0.99 for both metals. This suggests that chemisorption, involving electron exchange or sharing between the metal ions and PMCB, is the rate-limiting step. These findings align with previous studies and highlight our research's superior performance in achieving the highest adsorption capacities[51–53]. The Elovich kinetic model (Fig. S2c) provides insights into

the heterogeneity of the surface of PMCB and chemisorption. However, the R^2 for the Elovich model was less compared to the pseudo second-order model. Further analysis using multistage fitting of the intra-particle diffusion kinetic model, revealed discrete stages in the adsorption, as shown in Fig. S2d. The graph (Q_t vs. $t^{1/2}$) in Fig.S2d did not pass through the zero, depicting that the intra-particle diffusion kinetic model shows both rate-controlling step and boundary layer diffusion. The first stage is dominated by boundary layer diffusion, the second stage is dominated by intra-particle diffusion, and the third stage indicates equilibrium[54,55]. In this study, the observed rate constants ($K_{d1} > K_{d2}$) and equilibrium concentrations ($C_2 > C_1$) for both Cu^{2+} and Ni^{2+} removal on PMCB suggest a more efficient metal uptake during the initial stage compared to the subsequent phase[56]. Overall, the suitability of the kinetic models for Cu^{2+} and Ni^{2+} adsorption follows the order: pseudo-second order > intra-particle diffusion model > Elovich model > pseudo-first order.

The isotherm studies were conducted to characterize and quantify the adsorption capacity and mechanism of the adsorbent for specific adsorbates[57]. The calculated isotherm parameters are presented in Table S5, and the graphical analysis of these kinetic models is shown in Fig.S3. Fig.S3a illustrates a linear correlation between the adsorbate uptake (q) and the initial concentration (C_0) for both Cu^{2+} and Ni^{2+} ions onto the PMCB adsorbent. This linear isotherm behaviour suggests a homogeneous adsorption process, characteristic of monolayer coverage, where adsorbate molecules occupy discrete sites on the adsorbent surface without significant lateral interactions. To elucidate the underlying adsorption mechanism in greater detail, the experimental data can be fitted to established isotherm models such as Langmuir, Freundlich, and Temkin. This allows for the determination of model parameters and the assessment of their correlation coefficients[58,59]. The Freundlich model addresses heterogeneous adsorbent surfaces and multilayer adsorption. In this model, adsorption is favourable when 1/n is less than 1, cooperative when 1/n is greater than 1, and independent of concentration when 1/n equals 1[60]. The calculated 1/n values for Cu^{2+} and Ni^{2+} adsorption were 0.56 and 0.18, respectively, indicating a favourable adsorption process. Experimental data exhibited a moderate correlation with the model, evidenced by high R^2 values of 0.95 for Cu^{2+} and 0.96 for Ni^{2+}, as shown in Fig. S3b. The Langmuir isotherm, used for single-solute systems, assumes that all available sites on the monolayer adsorbent surface have equal adsorption capacity[28]. The PMCB adsorbent exhibited high adsorption capacities (q_{max}) of 564.97 mg/g for Cu^{2+} and 552.4 mg/g for Ni^{2+}, as shown in Table S5, indicating its strong affinity for the adsorbate. The calculated R_L values within the range of 0 to 1 suggest a favourable and spontaneous adsorption process. The excellent correlation between experimental data and the adsorption isotherm model, as evidenced by high R^2 values (0.97 and 0.98) in Fig. S3c, confirms the reliability of the findings. Similar trends were observed in the literature, with improved adsorption capacities for Cu^{2+} and Ni^{2+}[28,61,62]. The Temkin isotherm describes interactions on heterogeneous surfaces, proposing a decrease in the heat of adsorption as surface coverage increases[63]. This decrease, validated by thermodynamic studies, specifies that the adsorption is exothermic, with a good correlation between experimental data and the adsorption isotherm model, as evidenced by high R^2 values (0.96 and 0.987) in Fig. S3d. The Dubinin-Radushkevich (D-R) isotherm helps determine whether the adsorption process is physical or chemical, based on the mean free energy (E). An E value of < 8 kJ/mol specifies physical adsorption, while values between 20 and 40 kJ/mol suggest chemisorption and a range of 8–16 kJ/mol indicates an ion-exchange mechanism[64,65]. In this study, the E values were 2 kJ/mol for Ni^{2+} and 15.32 kJ/mol for Cu^{2+}, suggesting physical adsorption for Ni^{2+} and ion exchange for Cu^{2+} as shown in Fig. S3e. Analysis of adsorption isotherm models indicated that the Langmuir model exhibited the most favorable fit for both Cu^{2+} and Ni^{2+} adsorption, as evidenced by the highest adsorption capacity and correlation coefficients as R^2 is presented (0.98 and 0.99).

Impact of coexisting ions in different systems

Adsorbents to remove multiple contaminants from actual effluent have not been well discussed so far. Therefore, in this study, the performance of PMCB in simultaneously capturing various pollutants from single, multiple aqueous systems and industrial wastewater was investigated. The effluent composition was analyzed using XRF, while the concentration was determined by AAS, and the findings are presented in Table.S6. The influence of coexisting ions in single and multiple aqueous systems is explained in detail in Sec.S7 and Fig. 2e. Experimental conditions for the influence of coexisting ions in the real system include 3 g/L dosage, pH of 6, agitation at 180 rpm, and 100 mL effluent in a 250 mL beaker at room temperature. In the multi-ion system, the behaviour of each metal ion is influenced by its distinct ionic size, electronegativity, and charge[66–68]. Pb^{2+} ions with their large size and high charge density exhibit strong affinity for PMCB functional groups (carboxyl (-COOH), hydroxyl (-OH), and phosphate (PO_4^{3-})) resulting in significant adsorption. Cu^{2+}, possessing moderate size and high electronegativity, also form strong complexes with the surface of PMCB, leading to substantial removal from the solution. Ni^{2+}, with similar characteristics to Cu^{2+}, demonstrates effective complexation and electrostatic interactions, contributing to their notable adsorption capacity. As^{2+}, with moderate size and charge density, exhibits less completion towards Cu^{2+} and Ni^{2+}. Zn^{2+} which is smaller in size with a moderate charge density displays moderate adsorption due to electrostatic interactions and complexation among other metals. The PMCB exhibited remarkable performance by reducing Cu^{2+} concentrations from 984 mg/L to 1.5 mg/L and Ni^{2+} concentrations from 750 mg/L to 1.9 mg/L, achieving compliance with industrial wastewater standards with a removal efficiency of over 99% and shown in Fig. 2e1[69,70]. Additionally, PMCB effectively decreased the levels of most of the pollutants to acceptable limits, as detailed in Table S6. A comparison of heavy metal removal using PMCB in real systems with reported methods represented in Table 2. These results highlight the potential of PMCB as an advanced and versatile adsorbent, offering a significant improvement over traditional selective adsorption methods for treating real effluents.

Comparison of PMCB $Cu^{2+}$and Ni^{2+}removal with literature studies in batch mode			
Modified biochar	**Adsorption factors**	**Adsorption Capacity(mg/g)**	**Ref.**
Crab processing by-product biochar	Dosage = 5 g/L, pH = 7.1, t = 2 h, C_0 = 100 mg/L and T = 303 K	184.8 (Cu^{2+})	104
Juglans regia magnetic Biochar	Dosage = 3 g/L, pH = 6, t = 2 h, C_0 = 50 mg/L and T = 303 K	16.83 (Cu^{2+}) and 18.11 (Ni^{2+})	105
Coco nutshell biochar	Dosage = 5 g/L, pH = 5, t = 2 h, C_0 =80 mg/L and T = 298 K	89.0 (Cu^{2+})	4
Coconut coir	Dosage = 2.5 g/L, pH = 4.17, t = 3.4 h, C_0 =400 mg/L and T = 300 K	8.84 (Ni^{2+})	106
Jackfruit fruit biochar	Dosage = 3 g/L, pH = 6, t = 1.5 h, C_0 =50 mg/L and T = 333 K	52.06 (Ni^{2+})	107
Coco peat biomass	Dosage = 0.6 g/L, pH = 5 (Cu^{2+}), 6 (Ni^{2+}), t = 1 h, C_0 = 350 mg/L and T = 303 K	58 (Cu^{2+}) and 48 (Ni^{2+})	**Present study**
Coco peat biochar	Dosage = 0.6 g/L, pH = 5 (Cu^{2+}), 6 (Ni^{2+}), t = 1 h, C_0 = 350 mg/L and T = 303 K	95.4 (Cu^{2+}) and 85 (Ni^{2+})	**Present study**
Cocopeat H_3PO_4 treated biochar	Dosage = 0.6 g/L, pH = 5 (Cu^{2+}), 6 (Ni^{2+}), t = 1 h, C_0 = 350 mg/L and T = 303 K	564.85(Cu^{2+}) and 548.3 (Ni^{2+})	**Present study**
Comparison with literature studies on column mode			
Modified biochar	**Adsorption factors**	**Adsorption**	**Ref.**
Polyethylenimine modified wheat straw	C_0 = 10 mg/L, pH = 5, flow rate = 210 mL/h and Bed height = 10 cm	48.6 (Cu^{2+})	108
Neem leaf powder	C_0 = 5 mg/L for both metals, pH = 5, flow rate = 300 mL/h and Bed height = 20 cm	154.5 (Cu^{2+}) and 120.6 (Ni^{2+})	109
Almond shell	C_0 = 67.5 mg/L, pH = 5, flow rate = 180 mL/h and Bed height = 7 cm	2.39 (Cu^{2+})	110
Phoenix dactylifera bio char	C_0 = 20 mg/L for both metals, pH = 7, flow rate = 600 mL/h and Bed height = 1 cm	26.21 (Cu^{2+}) and 0.09 (Ni^{2+})	111
Poly(2-acrylamide-pentanedihydroxamic acid) resin	C_0 = 50 (Cu^{2+}) and 10 (Ni^{2+}) mg/L, pH = 7, flow rate = 120 mL/h and Bed height = 2 cm	436.08 (Cu^{2+}) and 15.08 (Ni^{2+})	112
PMCB	C_0 = 350 mg/L, pH = 5, flow rate = 600 mL/h and Bed height = 15 cm	794.5 (Cu^{2+}) and 691.4 (Ni^{2+})	**Present study**
Comparison of multi-metal removal with reported ones						
		Removal efficiency (%)				
Adsorbent	**Source of Pollutant**	**Cu^{2+}**	**Ni^{2+}**	**Zn^{2+}**		**Ref.**
Rice husk	Electroplating industry	24.5	94.8	-	-	113
Magnesium oxide nanoparticles	Textile and tannery effluent	-	70.80	-	-	114
Polyvinyl alcohol-modified chitosan	Battery effluent	79.1	50.7	46.9	-	115
Peanut husk powder	Industry Wastewater	51	24	38	100	3
PMCB	Battery effluent	99.8	99.7	99.6	99.4	**Present study**
Comparison of Cost analysis per kg production of PMCB with literature				
Adsorbent	**Adsorption capacity (mg/g)**	**Cost (USD/kg)**	**Ref.**
Titania/graphene oxide	168.067 (Cu^{2+})	46	116
Cherry kernels bio char	66.22 (Ni^{2+})	41.9	117
Rice straw biochar	35.71 (Zn^{2+})	2.6	118
Rice straw	32.81 (Zn^{2+})	0.55	119
PMCB	566.6 (Cu^{2+}), 551.7 (Ni^{2+}) and 178.2 (Zn^{2+})	1.56	**Present study**

Table 2. Comparison of PMCB Cu^{2+} and Ni^{2+}elimination with literature studies.

Column studies

Effect of column parameters

The effective utilization of adsorbents mainly depends on the consistent operation of fixed-bed columns, which is a critical aspect for determining the feasibility of the process. To assess the performance of fixed-bed columns, experiments were conducted on varying parameters like the height of the PMBC bed (ranging from 5 to 15 cm), the flow rate of the solution (600 to 1200 mL/h), and initial concentrations of copper and nickel (ranging from 100 to 350 mg/L). The effect of column parameters is explained in Sec.S8 and the results of these experiments are compiled in Tables S7, S8 and S9. By analyzing breakthrough curves obtained from these experiments, the uptake capacity in continuous mode was determined, leading to the insights discussed below.

Break-through curve modelling

Breakthrough curves are essential for the effective design and process optimization of adsorption columns. Thomas and Yoon-Nelson (YN) models were used to characterize the adsorption of copper and nickel onto PMBC[71,72]. The model equations and system factors used for scale-up in real applications are provided in Table S9. Thomas's model was employed to analyze continuous adsorption processes in a column and used to calculate both the kinetic factors and maximum uptake capacity. The results revealed that the adsorption capacity of the column (q_{Th}) increased with higher bed height and initial concentration, but decreased with increasing flow rate. This trend can be attributed to the fact that a taller bed provides a greater amount of adsorbent and a longer contact time, enhancing adsorption. Similarly, higher influent concentrations offer a stronger driving force for mass transfer, leading to more effective utilization of the adsorption sites. However, at higher flow

rates, the reduced residence time limits the interaction between adsorbate and adsorbent, resulting in lower capacity. In contrast, the Thomas rate constant (K_{Th}) was found to decrease with increasing bed height and initial concentration, but increased with higher flow rates. The decline in K_{Th} with bed height and concentration may be due to more gradual mass transfer and longer equilibrium attainment time in deeper beds or under high loading conditions. On the other hand, at higher flow rates, the rapid mass transport enhances the apparent kinetics, thus increasing the rate constant. The models' correlation and regression coefficients for the tested parameters indicated that the Thomas model best described the sorption process, which is consistent with findings by[73,74]. The YN kinetic model predicts the YN model rate constant (K_{YN}) and 50% break through time (T) from Table S9. It was observed that K_{YN} increases with increases in flow rate and concentration and decreases with bed height. In contract K_{YN} decreases with bed height.The Yoon-Nelson (YN) model estimates the rate constant (K_{YN}) and the 50% breakthrough time (T) as shown in Table S9. It was observed that K_{YN} increased with higher flow rate and initial concentration, but decreased with increasing bed height. This is because higher flow rates reduce contact time, leading to faster breakthrough. Similarly, higher concentrations accelerate saturation of adsorption sites, enhancing the breakthrough rate. In contrast, increasing bed height extends the mass transfer zone and contact time, allowing more gradual adsorption, which lowers the value of K_{YN}[73,74]. A quantitative valuation based on R^2 values preferred the Thomas model ($R^2 = 0.99$) over the YN model ($R^2 = 0.98$) from Fig. 3. Remarkably, at an initial feed concentration of 350 mg/L, a bed height of 15 cm, and a flow rate of 900 mL/h, the maximum uptake capacities for copper and nickel were 794.5 mg/g and 691.4 mg/g, respectively. Parallel trends with better results were observed by[29,44,45,75].

Physiochemical characterization of PMCB

The morphological characteristics of CB and PMCB were analyzed using SEM to examine their microstructures and macrostructures in detail. Images of the core structure of PMCB, both before and after adsorption, are shown in Fig. 4. The structure of CB differs from that of the PAT sample. In Fig. 4a, the lignocellulosic surface construction of CB appears rough and integrated at a temperature of 383 K. In contrast, Fig. 4a1 shows the surface of PMCB, which has an open-pored, flake-like texture. The surface morphology of PMCB reveals numerous flakes with small pores and cavities, which are conducive to metal uptake due to the acid treatment[76–78] at 823 K. Figure 4, a2-a3 shows PMCB after adsorption, showing occupied pores and fewer active sites. The majority of the pores on the surface of PMCB are filled with metal ions through adsorption, resulting in fewer pores compared to fresh PMCB. Additionally, the thickness of the flakes increased after adsorption, indicating that the adsorbent had reached its capacity and could no longer absorb additional metal ions. The surface area of PMCB also appeared to decrease post-adsorption, as the adsorbent had reached saturation. This was evidenced by the thick, dispersed structures with large pores, further confirmed by BET analysis.

Elemental analysis of CB, pre and post-adsorption PMCB were analysed by EDX. It was hypothesized by[19,79] that stimulating H_3PO_4 could lead to the development of a phosphate ($-PO_4^{3-}$) and phosphite ($-PO_3^{3-}$) bond thereby improving the stability of carbon structures and improving metal adsorption. The results depicted in Table.S2 reveal a notable rise in C and P content at specific pyrolysis temperatures and H_3PO_4 concentrations. This increase supports the hypothesis, highlighting the crucial roles of phosphorus and carbon in the adsorption of copper and nickel. However, this characterization was based solely on qualitative observations using SEM and EDX. Detailed measurements, including porosity, pore volume distribution, diameters, and surface area

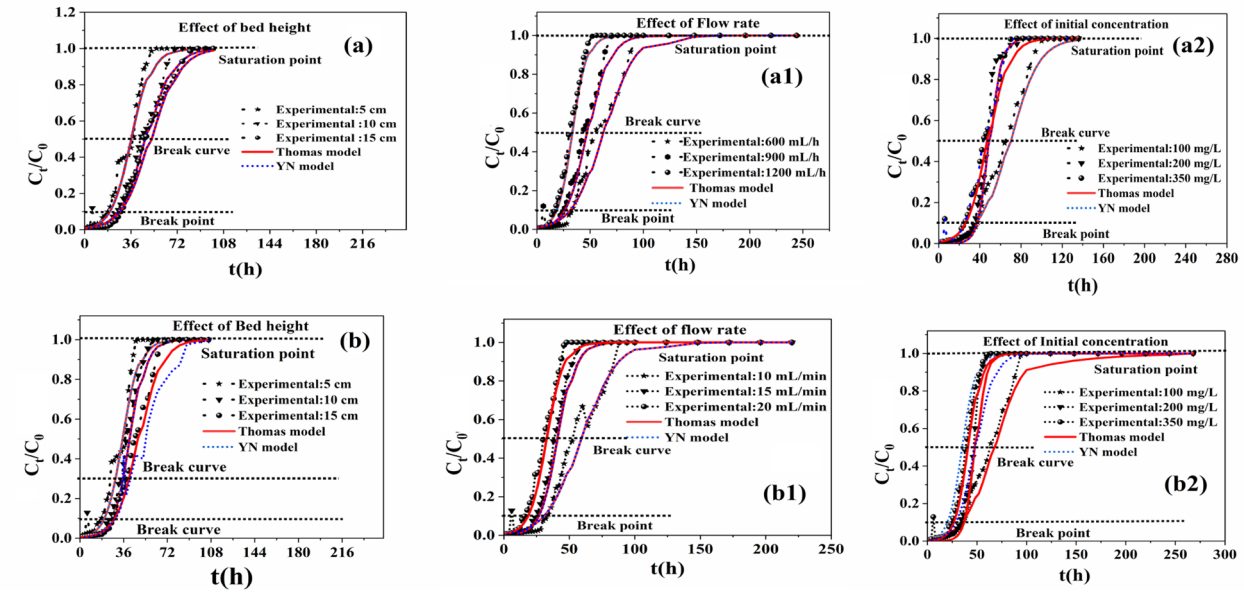

Fig. 3. Influence of operational parameters on column breakthrough curves for copper and nickel adsorption onto PMCB: **(a-b)** Effect of bed height, **(a1-b1)** Effect of flow rate, **(a2-b2)** Effect of initial concentration.

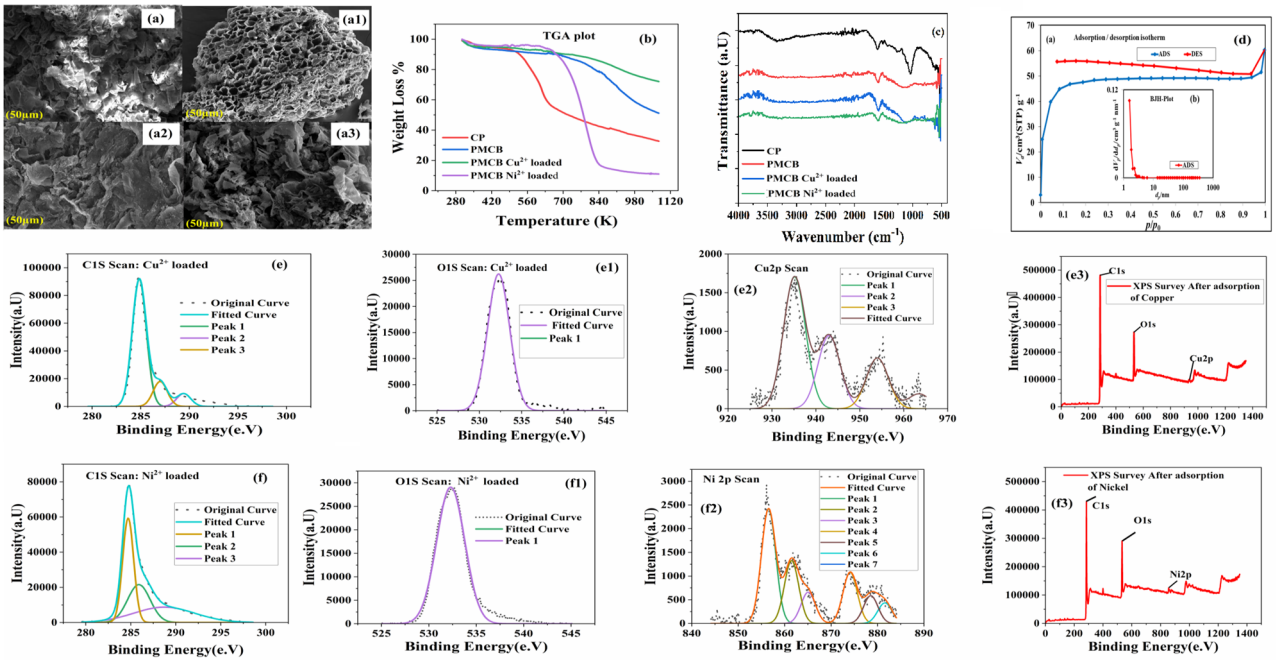

Fig. 4. Physiochemical characterization of PMCB before and after adsorption of Cu^{2+} and Ni^{2+}: (**a-a3**) SEM analysis (**b**) TGA analysis (**c**) FTIR analysis (**d**) BET analysis (**e-e3**) XPS analysis for Cu^{2+} adsorption (**f-f3**) XPS analysis for Ni^{2+} adsorption.

of the coco peat, are provided below further elucidating the significance of surface characteristics in enhancing sorption performance. The detailed analysis and explanation of TGA, FTIR and BET were explained in Sec.S9, represented in Fig. 4b, c, d and BET surface comparison of PMCB with other adsorbents represented in Table S.10.

XPS was utilized to analyze the elemental composition as well as the chemical and electronic state of atoms within CB and PMCB, both before and after the adsorption of Cu^{2+} and Ni^{2+}[80]. In Fig.S4, the C1s and O1s spectra of XPS for CB are presented. The C1s spectrum (Fig.S4a) shows a single peak at 284.48 eV, attributed to C = C. The O1s spectrum (Fig.S4b) displays a peak at 532.48 eV, indicating the presence of metal CO_3. Fig.S4c depicts the XPS survey scan of CB's elemental content. For PMCB, Fig.S5 illustrates the elemental content of C, P, and O with lower binding energy compared to CB due to pyrolysis. The C1s spectrum (Fig.S5a) shows three peaks such as C at 284.88 eV, carbonyl group at 286.78 eV, carboxylic group (O = C-O) at 288.2 eV, and carbonate group (CO_3^{2-}) at 289.2 eV[81]. Fig.S5b shows two peaks which peak one is phosphorous(V) pentaoxide at 532.60 e.V and peak 2 is sodium diphosphate at 533.40. Fig.S5c displays the P2p spectrum, indicating peaks corresponding to phosphate (PO_4^{3-}) at 132.2 eV and phosphorus pentoxide (P2O5) at 134.21 eV. This confirms the hypothesis proposed by[19,79] that the stimulation of H_3PO_4 could result in the formation of phosphate (PO_4^{3-})) bond, thereby enhancing the stability of carbon structures and improving metal adsorption. Fig.S5d displays the XPS survey scan of PMCB's elemental content. Figure 4e-e1 and 4f-f1 show the C1s spectra of PMCB with peaks at 284.78 eV, 287.2 eV (carboxylic group, O = C-O), and 289 eV (carbonate group, CO_3^{2-}), observed after the adsorption of Cu and Ni. The molar ratio of O = C-O, C-O and CO_3^{2-} improved significantly in the PMCB sample after adsorption, indicating the involvement of hydroxyl and carboxylic groups in heavy-metal removal which indicates surface complexation mechanism. The molar ratio of the C = O group on PMCB decreased after the adsorption of Cu and Ni ions. In Fig. 4e2, four peaks are observed, representing Cu^{2+}, $CuCO_3$, CuO, and $Cu_3(PO_4)_2$[82–84]. Figure 4e3 shows the XPS survey scan of PMCB after copper adsorption. Figure 4f2 displays seven peaks corresponding to Ni^{2+}, NiO, $Ni_3(PO_4)_2$, Ni^0, NiOOH, and $Ni(OH)_2$, after nickel adsorption, while Fig. 4f3 shows the XPS survey scan of PMCB after nickel[85,86]. XPS Simplified and the National Institute of Standards and Technology (NIST) database were taken for XPS analysis of CB and PMCB before and after the adsorption of Cu^{2+} and Ni^{2+}.

Adsorption mechanism

Biomass-based biochar is a versatile material which can be chemically altered to enhance its affinity towards metal ion adsorption[16]. XPS examination could detect the phosphate (PO_4^{3-}) and phosphorus pentoxide (P_2O_5) on PMCB following H_3PO_4 modification[87–89]. A comprehensive investigation of PMCB revealed two types of adsorption processes such as surface diffusion, intra-particle diffusion and five types of adsorption mechanisms which were illustrated in Fig. 5 including (1) ion exchange, (2) electrostatic interactions, (3) surface adsorption, (4) precipitation, and (5) surface complexation. The adsorption process begins with ion exchange, where copper and nickel ions replace other ions on the biochar surface, effectively immobilizing them. Phosphoric acid modification introduces carboxyl, hydroxyl, and carbonyl functional groups onto the biochar matrix. These oxygen-containing groups impart a negative surface charge, facilitating the electrostatic attraction of

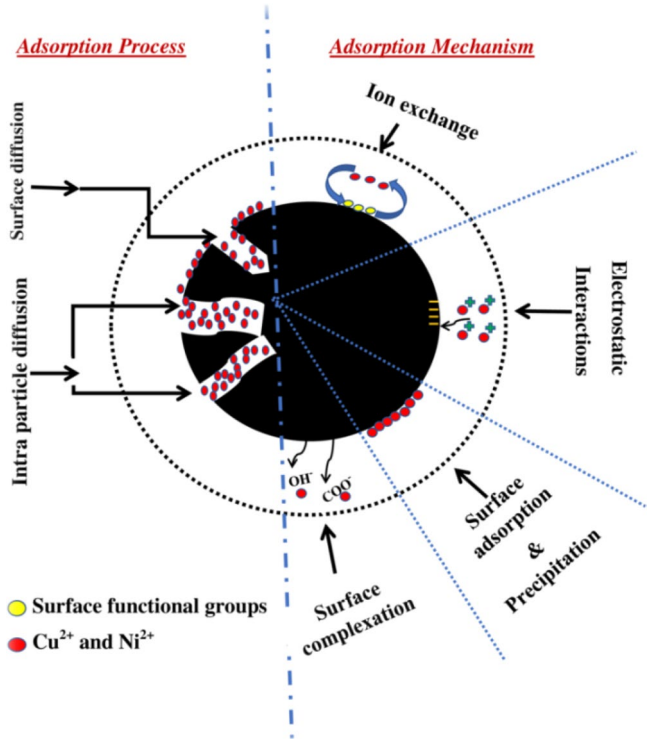

Fig. 5. Pictorial representation of adsorption processes and mechanisms during copper and nickel removal by PMCB.

divalent cations such as copper and nickel. Subsequent surface complexation reactions between the metal ions and functional groups enhance the sequestration capacity of the biochar for these pollutants. This process was validated through XPS binding energy values and FTIR analysis[90–92]. At pH levels above 6, Cu^{2+} and Ni^{2+} ions precipitate as insoluble compounds, specifically $Cu_3(PO_4)_2$ and $Ni_3(PO_4)_2$, as confirmed by the pH study and validated by XPS analysis. The negative ΔH^0 and ΔS^0 values indicate that the adsorption of Cu^{2+} and Ni^{2+} on PMCB is an exothermic, spontaneous process driven by physisorption with decreased randomness at the solid–solution interface. Kinetic studies showed that the pseudo-second order could best fit the data, indicating the occurrence of chemisorption. BET and SEM analyses revealed numerous micropores on the surface of PMCB, suggesting that the surface diffusion phenomenon was predominant. The intra-particle diffusion model indicated that the adsorption process involved both the rate-controlling step within the porous material (intra-particle diffusion) and the transport of solute molecules from the bulk solution to the material's surface (boundary layer diffusion) for both metals[91,93].

Regeneration, reuse and cost analysis studies

Regeneration studies

Regenerating adsorbents by desorbing the adsorbed metal ions under suitable conditions is crucial for enabling repeated use and reducing material costs[24,26]. To delve into this, regeneration experiments were conducted with a contact time of 1.5 h, initial copper and nickel concentrations of 350 mg/L, at a temperature of 303 K, a pH of 6 and a stirring speed of 180 rpm. Various eluting agents (0.4 M solutions of H_2SO_4, HCl, HNO_3, and distilled water (DI water) were tested and presented in (Fig. 6a). Among these, 0.4 M H_2SO_4 demonstrated the highest desorption efficiency. To find the optimal concentration of H_2SO_4, experiments were carried out with varying concentrations from 0.1 M to 1 M. The results indicated that 0.6 M H_2SO_4 provided the highest desorption efficiency (Fig. 6b). However, increasing the concentration to 0.8 to 1 M resulted in precipitation. Based on these findings, 0.6 M H_2SO_4 was selected for further studies. To assess PMCB's stability and regenerative capacity, adsorption-desorption cycles were repeated under identical process conditions. PMCB exhibited the potential for adsorption for up to 20 desorption cycles which is shown in Fig. 6c. Desorption of both ions from PMCB exhibited an efficiency of 98.6% and 96.0%, respectively and the detailed table with adsorption capacity values mentioned in Table S11.

Spent Biochar as a biofertilizer to prevent secondary pollution

From reported studies of heavy metal removal using biomass based adsorbents, it could be observed that very little focus was laid on developing an effective reuse strategy of the spend adsorbent which could be critical for sustainable and circular economy. Few studies have investigated the conversion of biomass and char into briquettes[94,95]. However, the no attempt was made to use spent phosphoric acid-modified biochar (PMCB) as a soil amendment biofertilizer[56,96]. In this study, three types of soil mixtures were used in terms of their response

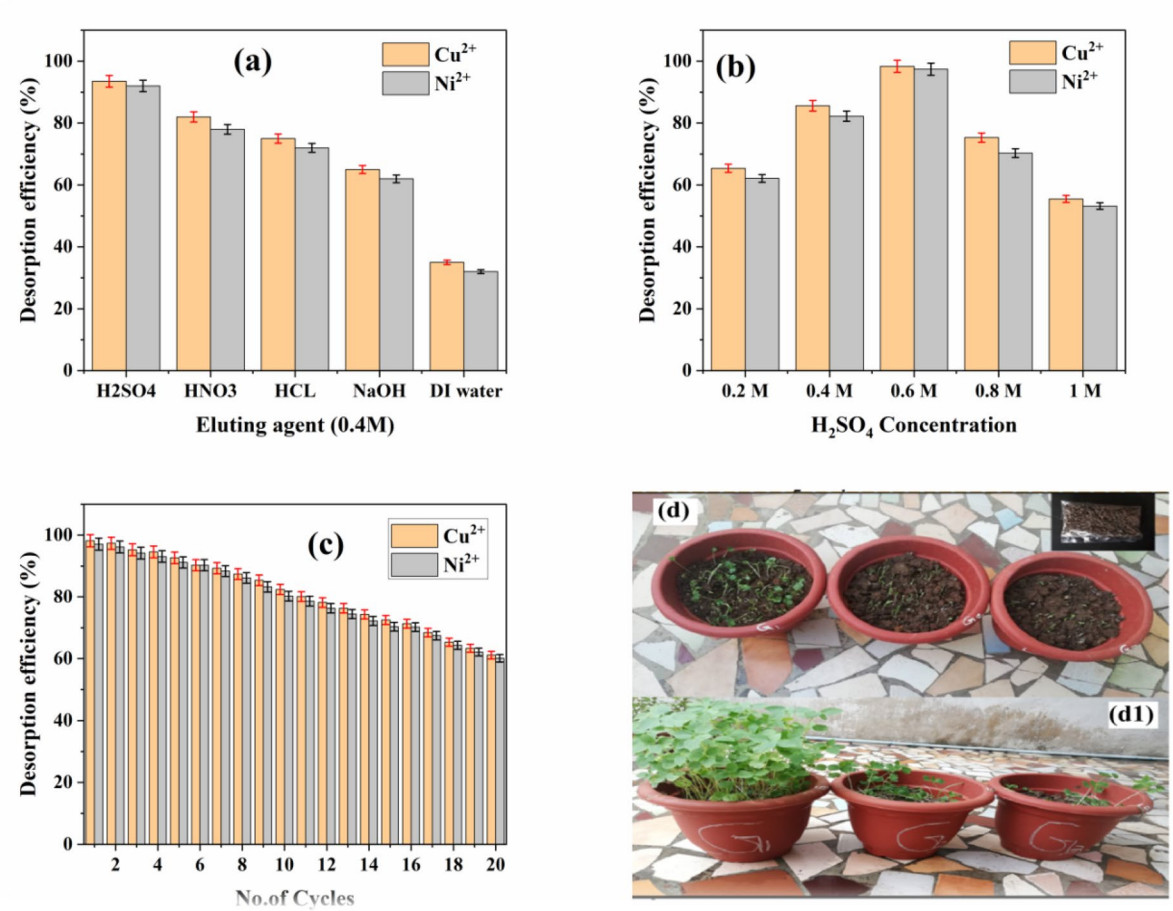

Fig. 6. **(a-c)** illustrates the regeneration studies on Cu^{2+} and Ni^{2+}**(a)** Selection of eluting agent **(b)** Selection of optimum H_2SO_4 concentration **(c)** Cyclic studies of PMCB candidate, and **(d-d1)** illustrates the impact of spent PMCB on plant development using soil mixtures: G_1 (soil + spent biochar), G_2 (soil + NPK), and G_3 (pure soil), focusing on **(d)** Seed germination and **(d1)** Shoot length.

to promote the growth of sorrel (*Gongura*). Three plastic pots G_1, G_2, and G_3 presented in Fig. 6d, represent soil mixed with spent biochar (G_1), soil mixed with NPK (G_2) and regular soil (G_3). The results clearly indicated that incorporating spent PMCB into the soil (pot G_1) resulted in quicker seed germination and improved plant growth compared to pots G_2 and G_3 as shown in Fig. 6d. Additionally, the biochar incorporated soil in pot G_1 demonstrated superior shoot strength and growth compared to pots G_2 and G_3 as shown in Fig. 6d1. After one week, this improved performance could be attributed to the biochar's phosphorus content (H_3PO_4 treatment), which served as a vital nutrient for the plant growth[97]. But caution was needed before these plans could be used for human consumption as they were grown using soil with spent biochar having heavy metals. More advanced studies are recommended in this direction[98,99]. However it proposed that soils possessed with heavy metals could serve as suitable environment for cultivating decorative plants[100,101]. The resulting plant biomass could be repurposed for various applications such as air fresheners, cut flowers, perfumes, metal phytomining, and as feedstock for silk production. Moreover, these plants pose a lower risk of heavy metal bioaccumulation compared to traditional crops. Based on these findings, there is a great potential for spent PMCB to be utilized as a biofertilizer in pot plant systems, which are increasingly becoming popular in malls, offices, and institutions as indoor gardens. More technical studies were needed to validate this conclusion.

Cost analysis of PMCB Preparation

The abundant production of coconut in southern India provides a rich source of raw materials, making biochar a promising solution for heavy metal remediation. Evaluating the cost of making biochar is essential for assessing its viability as an engineered solution for removing heavy metals from wastewater[102,103]. In addition to the assessment of PMCB's efficacy in eliminating both metals from wastewater, cost analysis of producing engineered biochar from coconut waste was explored. The cost analysis for 1 kg PMCB production is explained in detail in Sec.S10 and Fig.S6. The comparison of the cost of PMCB production over commercially available candidates is presented in Table 2.

Comprehensive comparison of PMCB with literature

PMCB exhibits superior performance in batch mode, column mode, multimetal systems, and cost analysis, outperforming many previously reported results as shown in Table 2.

Conclusions

From the findings, it could be concluded that H_3PO_4-modified biochar (PMCB) was an effective adsorbent for heavy metal removal, having been identified through a rigorous three-tier screening process. By optimizing the synthesis conditions (0.6 M H_3PO_4 concentration and a pyrolysis temperature of 823 K), PMCB exhibited enhanced physicochemical properties, resulting in high adsorption capacities for Cu^{2+} (566.6 mg/g in batch tests and 794.5 mg/g in column studies) and Ni^{2+} (551.7 mg/g in batch tests and 691.4 mg/g in column studies). PMCB demonstrated over 99% removal efficiency for these heavy metals in both synthetic and real effluent systems. Additionally, PMCB exhibited impressive stability with reusability for up to 20 cycles and a 96.0% desorption rate, with the spent biochar showing a good potential as a bio-fertilizer. Cost analysis further supported the viability of PMCB, with a production cost of just 1.56 USD/kg (130.7 INR/kg), indicating its potential as a sustainable, cost-effective solution for industrial heavy metal removal from wastewaters.

Data availability

All data generated or analysed during this study are included in this published work (and the supplementary information files).

Received: 13 March 2025; Accepted: 16 September 2025
Published online: 23 October 2025

References

1. Indhumathi, P. et al. The efficient removal of heavy metal ions from industry effluents using waste biomass as Low-Cost adsorbent: thermodynamic and kinetic models. *Zeitschrift Fur Phys. Chemie* **232**, (4) 527–543 (2018).
2. Sireesha, S. & Sreedhar, I. Modified low cost engineered Biochar prepared from Neem de-oiled cake for heavy metal sorption. *Mater. Today Proc.* **72**, 34–40 (2022).
3. Abdelfattah, I., Ismail, A. A., Sayed, F., Al, Almedolab, A. & Aboelghait, K. M. Biosorption of heavy metals ions in real industrial wastewater using peanut husk as efficient and cost effective adsorbent. *Environ. Nanatechnol. Monit. Manag* **6**, 176–183 (2016).
4. Gupta, S., Sireesha, S., Sreedhar, I., Patel, C. M. & Anitha, K. L. Latest trends in heavy metal removal from wastewater by Biochar based sorbents. *J. Water Process. Eng.* **38**, 101561 (2020).
5. Lin, G. et al. A systematic review of metal organic frameworks materials for heavy metal removal: Synthesis, applications and mechanism. *Chem. Eng. J.* **460**, 141710 (2023).
6. Iwuozor, K. O. Prospects and challenges of using Coagulation-Flocculation method in the treatment of effluents. *Adv. J. Chem. A.* **2**, 105127 (2019).
7. Khandgave, S. S. & Sreedhar, I. A mini-review on engineered biochars as emerging adsorbents in heavy metal removal. *Mater. Today Proc.* **72**, 19–26 (2022).
8. Ismail, U. M., Vohra, M. S. & Onaizi, S. A. Adsorptive removal of heavy metals from aqueous solutions: progress of adsorbents development and their effectiveness. *Environ. Res.* **251**, 118562 (2024).
9. Al-Shannag, M. et al. On the performance of Ballota undulata biomass for the removal of cadmium(II) ions from water. *Desalin. Water Treat.* **67**, 223–230 (2017).
10. Yao, B., Zeng, W., Núñez-Delgado, A. & Zhou, Y. Simultaneous adsorption of Ciprofloxacin and Cu2 + using Fe and N co-doped biochar: competition and selective separation. *Waste Manag.* **168**, 386–395 (2023).
11. Ogata, F., Nagai, N., Itami, R., Nakamura, T. & Kawasaki, N. Potential of Virgin and calcined wheat Bran biomass for the removal of chromium(VI) ion from a synthetic aqueous solution. *J. Environ. Chem. Eng.* **8**, 103710 (2020).
12. Ajien, A., Idris, J., Md Sofwan, N., Husen, R. & Seli, H. Coconut shell and husk biochar: A review of production and activation technology, economic, financial aspect and application. *Waste Manag Res.* **41**, 37–51 (2023).
13. Xu, H. et al. Journal of environmental chemical engineering enhanced removal efficiency of cd $^{2+}$ and Pb $^{2+}$ from aqueous solution by H_3PO_4 – modified tea branch biochar: Characterization, adsorption performance and mechanism. *J. Environ. Chem. Eng.* **12**, 112183 (2024).
14. Agarwal, A., Upadhyay, U., Sreedhar, I., Singh, S. A. & Patel, C. M. A review on valorization of biomass in heavy metal removal from wastewater. *J. Water Process. Eng.* **38**, 101602 (2020).
15. Han, S. et al. Preparation of modified Reed carbon composite hydrogels for trapping Cu2+, Ni2 + and methylene blue in aqueous solutions. *J. Colloid Interface Sci.* **628**, 878–890 (2022).
16. Guo, C. et al. Organic pollutants removal by phosphoric acid modified Biochar from residue of inonotus obliquus. *J. Environ. Chem. Eng.* **11**, 110292 (2023).
17. Sajjadi, B., Chen, W. Y., Mattern, D. L., Hammer, N. & Dorris, A. Low-temperature acoustic-based activation of Biochar for enhanced removal of heavy metals. *J. Water Process. Eng.* **34**, 101166 (2020).
18. Elmouwahidi, A., Bailón-García, E., Pérez-Cadenas, A. F., Maldonado-Hódar, F. J. & Carrasco-Marín, F. Activated carbons from KOH and H3PO4-activation of Olive residues and its application as supercapacitor electrodes. *Electrochim. Acta.* **229**, 219–228 (2017).
19. Dechapanya, W. & Khamwichit, A. Biosorption of aqueous Pb(II) by H3PO4-activated Biochar prepared from palm kernel shells (PKS). *Heliyon* **9**, e17250 (2023).
20. Bahsaine, K. et al. Efficient cadmium removal from industrial phosphoric acid using banana pseudostem-derived Biochar. *Biomass Convers. Biorefinery*. **14**, 17745–17759 (2023).
21. Thabede, P. M., Shooto, N. D., Xaba, T. & Naidoo, E. B. Adsorption studies of toxic cadmium(II) and chromium(VI) ions from aqueous solution by activated black Cumin (Nigella sativa) seeds. *J. Environ. Chem. Eng.* **8**, 104045 (2020).
22. Jia, X. et al. Mesopore-rich badam-shell Biochar for efficient adsorption of Cr(VI) from aqueous solution. *J. Environ. Chem. Eng.* **9**, 105634 (2021).
23. Islam, M. S., Roy, H. & Afrose, S. Phosphoric acid surface modified Moringa Oleifera leaves Biochar for the sequestration of Methyl orange from aqueous solution: Characterizations, isotherm, and kinetics analysis. *Remediation* **32**, 281–298 (2022).
24. Wang, Z. Phosphorus-modified bone Chars with developed porosity for efficient removal of Pb(II), Cu(II), and Cd(II). *Environ. Sci. Pollut Res. Int.* **30**, 123796–123807 (2023).
25. Razak, M. R. et al. Phosphoric acid modified Kenaf fiber (K-PA) as green adsorbent for the removal of copper (II) ions towards industrial waste water effluents. *React. Funct. Polym.* **147**, 104466 (2020).

26. Meng, X. & Hu, R. Nitrogen/phosphorus enriched Biochar with enhanced porosity activated by guanidine phosphate for efficient passivation of Pb(II), Cu(II) and Cd(II). *J. Mol. Liq.* **323**, 115071 (2021).
27. Liu, C., Lin, J., Chen, H., Wang, W. & Yang, Y. Comparative study of Biochar modified with different functional groups for efficient removal of Pb(II) and Ni(II). *Int. J. Environ. Res. Public. Health.* **19**, 11163 (2022).
28. Upadhyay, U., Sireesha, S., Gupta, S., Sreedhar, I. & Anitha, K. L. Freeze v/s air-dried alginate-pectin gel beads modified with sodium Dodecyl sulphate for enhanced removal of copper ions. *Carbohydr. Polym.* **301**, 120294 (2023).
29. Ravindiran, G. et al. Conversion of seaweed waste to Biochar for the removal of heavy metal ions from aqueous solution: A sustainable method to address eutrophication problem in water bodies. *Environ. Res.* **241**, 117551 (2024).
30. Khan, N., Wahid, F., Sultana, Q., Saqib, N. U. & Rahim, M. Surface oxidized and un-oxidized activated carbon derived from Ziziphus jujube Stem, and its application in removal of Cd(II) and Pb(II) from aqueous media. *SN Appl. Sci.* **2**, 1–11 (2020).
31. Trikkaliotis, D. G., Christoforidis, A. K., Mitropoulos, A. C. & Kyzas, G. Z. Adsorption of copper ions onto chitosan/poly(vinyl alcohol) beads functionalized with poly(ethylene glycol). *Carbohydr. Polym.* **234**, 115890 (2020).
32. Salman, M. S. et al. Improving copper(II) ion detection and adsorption from wastewater by the ligand-functionalized composite adsorbent. *J. Mol. Struct.* **1282**, 135259 (2023).
33. Rasee, A. I. et al. Efficient separation, adsorption, and recovery of Samarium(III) ions using novel ligand-based composite adsorbent. *Surf. Interfaces.* **41**, 103276 (2023).
34. Han, Y. et al. Integrated machine learning and response surface methodology for screening and optimization of high-performance Mg-modified bamboo Biochar for phosphorus adsorption in water. *Ind. Crops Prod.* **231**, 121213 (2025).
35. Gong, W. et al. Adsorption of phosphorus in wastewater by lanthanum-modified magnetic sewage sludge Biochar. *Desalin. Water Treat.* **320**, 100603 (2024).
36. Biswas, B. et al. Phosphorus adsorption using chemical and metal chloride activated biochars: Isotherms, kinetics and mechanism study. *Heliyon* **9**, e19830 (2023).
37. Cai, Y., Jiang, W., Liu, D. & Chang, C. Adsorption of sulfanilamides using Biochar derived from Suaeda salsa: adsorption kinetics, isotherm, thermodynamics, and mechanism. *Environ. Sci. Pollut Res.* **30**, 70528–70540 (2023).
38. Katiyar, R. et al. Bioresource technology adsorption of copper (II) in aqueous solution using biochars derived from ascophyllum nodosum seaweed. *Bioresour Technol.* **328**, 124829 (2021).
39. Sheikh, M. C. et al. Toxic cadmium(II) monitoring and removal from aqueous solution using ligand-based facial composite adsorbent. *J. Mol. Liq.* **389**, 122854 (2023).
40. Sahmoune, M. N. Evaluation of thermodynamic parameters for adsorption of heavy metals by green adsorbents. *Environ. Chem. Lett.* **17**, 697–704 (2019).
41. Samuel, M. S., Selvarajan, E., Chidambaram, R., Patel, H. & Brindhadevi, K. Clean approach for chromium removal in aqueous environments and role of nanomaterials in bioremediation: present research and future perspective. *Chemosphere* **284**, 131368 (2021).
42. Ezeonuegbu, B. A. et al. Agricultural waste of sugarcane Bagasse as efficient adsorbent for lead and nickel removal from untreated wastewater: Biosorption, equilibrium isotherms, kinetics and desorption studies. *Biotechnol. Rep.* **30**, e00614 (2021).
43. Kumar, P. S. et al. Adsorption behavior of nickel(II) onto cashew nut shell: Equilibrium, thermodynamics, kinetics, mechanism and process design. *Chem. Eng. J.* **167**, 122–131 (2011).
44. Atugoda, T., Gunawardane, C., Ahmad, M. & Vithanage, M. Mechanistic interaction of Ciprofloxacin on zeolite modified seaweed (Sargassum crassifolium) derived biochar: Kinetics, isotherm and thermodynamics. *Chemosphere* **281**, 130676 (2021).
45. Njaramba, L. K. et al. Remarkable adsorption for hazardous organic and inorganic contaminants by multifunctional amorphous core–shell structures of metal–organic framework-alginate composites. *Chem. Eng. J.* **431**, 133415 (2022).
46. Wang, H. et al. Adenosine-functionalized UiO-66-NH2 to efficiently remove Pb(II) and Cr(VI) from aqueous solution: Thermodynamics, kinetics and isothermal adsorption. *J. Hazard. Mater.* **425**, 127771 (2022).
47. El-Khaiary, M. I. Least-squares regression of adsorption equilibrium data: comparing the options. *J. Hazard. Mater.* **158**, 73–87 (2008).
48. González-lópez, M. E. et al. A critical overview of adsorption models linearization: methodological and statistical inconsistencies A critical overview of adsorption models linearization : methodological and. *Separation and Purification Reviews***51**, 358–372 (2021).
49. Ajmani, A., Patra, C., Subbiah, S. & Narayanasamy, S. Packed bed column studies of hexavalent chromium adsorption by zinc chloride activated carbon synthesized from phanera vahlii fruit biomass. *J. Environ. Chem. Eng.* **8**, 103825 (2020).
50. Sharma, D. N. & Yadav, A. Effective removal of Ni(II) ions from its aqueous solution by utilizing euphorbia thymifolia as an adsorbent. *Environ. Sci. Pollut Res.* **30**, 98787–98795 (2023).
51. Shafiq, M., Alazba, A. A. & Amin, M. T. Kinetic and isotherm studies of ni2 + and pb2 + adsorption from synthetic wastewater using Eucalyptus camdulensis—derived Biochar. *Sustain* **13**, 3785 (2021).
52. El-Nemr, M. A., Abdelmonem, N. M., Ismail, I. M. A., Ragab, S. & El Nemr, A. Ozone and ammonium hydroxide modification of Biochar prepared from Pisum sativum peels improves the adsorption of copper (II) from an aqueous medium. *Environ. Processes.* **7**, 97–1007 (2020).
53. Isaac, R. & Siddiqui, S. Sequestration of Ni(II) and Cu(II) using FeSO4 modified Zea Mays husk magnetic biochar: Isotherm, kinetics, thermodynamic studies and RSM. *J. Hazard. Mater. Adv.* **8**, 100162 (2022).
54. Farnane, M. et al. Alkaline treated Carob shells as sustainable biosorbent for clean recovery of heavy metals: Kinetics, equilibrium, ions interference and process optimisation. *Ecol. Eng.* **101**, 9–20 (2017).
55. Joseph, I. V., Tosheva, L. & Doyle, A. M. Simultaneous removal of Cd(II), Co(II), Cu(II), Pb(II), and Zn(II) ions from aqueous solutions via adsorption on FAU-type zeolites prepared from coal fly Ash. *J. Environ. Chem. Eng.* **8**, 103895 (2020).
56. Chu, G. et al. Phosphoric acid pretreatment enhances the specific surface areas of biochars by generation of micropores. *Environ. Pollut.* **240**, 1–9 (2018).
57. Katiyar, R. et al. Adsorption of copper (II) in aqueous solution using biochars derived from ascophyllum nodosum seaweed. *Bioresour Technol.* **328**, 124829 (2021).
58. El Mansouri, F. et al. Rapid elimination of copper (II), nickel (II) and chromium (VI) ions from aqueous solutions by charcoal modified with phosphoric acid used as a green biosorbent. *Polym. Adv. Technol.* **33**, 2254–2264 (2022).
59. Mondal, S. & Majumder, S. K. Honeycomb-like porous activated carbon for efficient copper (II) adsorption synthesized from natural source: kinetic study and equilibrium isotherm analysis. *J. Environ. Chem. Eng.* **7**, 103236 (2019).
60. Liu, X. et al. Optimization and mechanisms of biosorption process of Zn(II) on rape straw powders in aqueous solution. *Environ. Sci. Pollut Res.* **26**, 32151–32164 (2019).
61. Batool, A., Munir, R., Mushtaq, N. & Noreen, S. Synthesis and comparison of different metal-doped ZnO nanoparticles for catalytic degradation and adsorptive removal of direct orange: kinetics, isotherms, and thermodynamics. *J. Sol-Gel Sci. Technol.* **112**, 240–261 (2024).
62. Georgieva, V. G., Gonsalvesh, L. & Tavlieva, M. P. Thermodynamics and kinetics of the removal of nickel (II) ions from aqueous solutions by Biochar adsorbent made from agro-waste walnut shells. *J. Mol. Liq.* **312**, 112788 (2020).
63. Bingül, Z. Determination of affecting parameters on removal of methylene blue dyestuff from aqueous solutions using natural clay: Isotherm, kinetic, and thermodynamic studies. *Journal of Molecular Structure***1250**,131729 (2022).
64. Chen, S. et al. Study on the adsorption of dyestuffs with different properties by sludge-rice husk biochar: adsorption capacity, isotherm, kinetic, thermodynamics and mechanism. *J. Mol. Liq.* **285**, 62–74 (2019).

65. Chen, S. et al. Study on adsorption of Cu2+, Pb2+, Cd2+, and Zn2 + by the KMnO4 modified Biochar derived from walnut shell. *Int. J. Environ. Sci. Technol.* **20**, 1551–1568 (2023).
66. Lee, H. S. & Shin, H. S. Competitive adsorption of heavy metals onto modified Biochars: comparison of Biochar properties and modification methods. *J. Environ. Manage.* **299**, 113651 (2021).
67. Wu, Q., Dong, S., Wang, L. & Li, X. Single and competitive adsorption behaviors of cu2+, pb2 + and zn2 + on the Biochar and magnetic Biochar of pomelo Peel in aqueous solution. *Water (Switzerland)* **13**, 868 (2021).
68. Ni, B. J. et al. Competitive adsorption of heavy metals in aqueous solution onto Biochar derived from anaerobically digested sludge. *Chemosphere* **219**, 351–357 (2019).
69. Li, Q. et al. Progress in the treatment of copper(II)-containing wastewater and wastewater treatment systems based on combined technologies: A review. *J. Water Process. Eng.* **58**, 104746 (2024).
70. Manne, R., Kumaradoss, M. M. R. M., Iska, R. S. R., Devarajan, A. & Mekala, N. Water quality and risk assessment of copper content in drinking water stored in copper container. *Appl. Water Sci.* **12**, 1–8 (2022).
71. Kumar, P. et al. Enhanced copper (II) bioremediation from wastewater using nano magnetite (Fe3O4) modified Biochar of ascophyllum nodosum. *Bioresour Technol.* **388**, 129654 (2023).
72. Wang, H. et al. Black liquor as biomass feedstock to prepare zero-valent iron embedded Biochar with red mud for Cr(VI) removal: mechanisms insights and engineering practicality. *Bioresour Technol.* **311**, 123553 (2020).
73. Syeda, H. I., Muthukumaran, S. & Baskaran, K. Dynamic adsorption of heavy metals on functionalized and regeneratable biopolymeric aerogels: Fixed-bed column reactor modelling and dual functionality elution technique. *Sep. Purif. Technol.* **363**, 131861 (2025).
74. Rahman, M. M. et al. Adsorptive removal of toxic heavy metal and dyes from wastewater by rice husk (lignocellulosic biomass) derived activated biochar: A fixed-bed column adsorption study. *Carbohydr. Polym. Technol. Appl.* **9**, 100698 (2025).
75. Sireesha, S. & Sreedhar, I. Holistic and parametric optimization study on Cr(VI) removal using acid-treated Coco peat Biochar adsorbent. *Bioresour Technol. Rep.* **22**, 101486 (2023).
76. Zhao, N. et al. Adsorption and coadsorption mechanisms of Cr(VI) and organic contaminants on H3PO4 treated Biochar. *Chemosphere* **186**, 422–429 (2017).
77. Chen, Q., Zhang, T. C., Ouyang, L. & Yuan, S. Single-Step hydrothermal synthesis of Biochar from H3 PO4-Activated lettuce waste for efficient adsorption of Cd(II) in aqueous solution. *Molecules* **27**, 269 (2022).
78. Khadem, M. et al. Removal of heavy metals from wastewater using low-cost Biochar prepared from jackfruit seed waste. *Biomass Convers. Biorefinery.* **13**, 14447–14456 (2023).
79. Valero-Romero, M. J., García-Mateos, F. J., Rodríguez-Mirasol, J. & Cordero, T. Role of surface phosphorus complexes on the oxidation of porous carbons. *Fuel Process. Technol.* **157**, 116–126 (2017).
80. Xu, H. et al. Enhanced removal efficiency of Cd2 + and Pb2 + from aqueous solution by H3PO4–modified tea branch biochar: Characterization, adsorption performance and mechanism. *J. Environ. Chem. Eng.* **12**, 112183 (2024).
81. Ahamad, T., Naushad, M., Al-Saeedi, S. I., Almotairi, S. & Alshehri, S. M. Fabrication of MoS2/ZnS embedded in N/S doped carbon for the photocatalytic degradation of pesticide. *Mater. Lett.* **263**, 127271 (2020).
82. Liang, G. et al. Effective removal of carbamazepine and diclofenac by CuO/Cu2O/Cu-biochar composite with different adsorption mechanisms. *Environ. Sci. Pollut Res.* **27**, 45435–45446 (2020).
83. Suman, S. Conversion of solid biomass into biochar: act as a Green, Eco-Friendly energy source and a substitute of fossil fuel inputs. *Proceedings***58**,34 (2020).
84. Bandara, T. et al. Mechanisms for the removal of Cd(II) and Cu(II) from aqueous solution and mine water by biochars derived from agricultural wastes. *Chemosphere* **254**, 126745 (2020).
85. Wu, J., Yi, Y. Q., Li, Y. Q., Fang, Z. & Tsang, E. P. Excellently reactive Ni/Fe bimetallic catalyst supported by Biochar for the remediation of Decabromodiphenyl contaminated soil: Reactivity, mechanism, pathways and reducing secondary risks. *J. Hazard. Mater.* **320**, 341–349 (2016).
86. Guan, B. et al. Synthesis of hierarchical NiS microflowers for high performance asymmetric supercapacitor. *Chem. Eng. J.* **308**, 1165–1173 (2017).
87. Ning, Z. et al. Preparation of phosphoric acid modified antibiotic mycelial residues biochar: loading of nano zero-valent iron and promotion on biogas production. *Bioresour Technol.* **348**, 126801 (2022).
88. Ibrahim, Z. et al. Adsorption of pyridine onto activated montmorillonite clays: effect Factors, adsorption behavior and mechanism study. *Am. J. Anal. Chem.* **09**, 464–481 (2018).
89. Zeng, H. et al. Efficient adsorption of cr (VI) from aqueous environments by phosphoric acid activated Eucalyptus Biochar. *J. Clean. Prod.* **286**, 124964 (2021).
90. Akhavan, O., Ghaderi, E., Emamy, H. & Akhavan, F. Genotoxicity of graphene nanoribbons in human mesenchymal stem cells. *Carbon N Y.* **54**, 419–431 (2013).
91. Peng, H. et al. Enhanced adsorption of Cu(II) and Cd(II) by phosphoric acid-modified biochars. *Environ. Pollut.* **229**, 846–853 (2017).
92. Xue, Y. et al. Hydrogen peroxide modification enhances the ability of Biochar (hydrochar) produced from hydrothermal carbonization of peanut hull to remove aqueous heavy metals: batch and column tests. *Chem. Eng. J.* **200–202**, 673–680 (2012).
93. Ateş, A., Mert, Y. & Timko, M. T. Evaluation of characteristics of raw tea waste-derived adsorbents for removal of metals from aqueous medium. *Biomass Convers. Biorefinery. 13,7811–7826* (2021).
94. Ali, A. et al. Insight into the Biomass-Based briquette generation from Agro-Residues: Challenges, Perspectives, and innovations. *Bioenergy Res.* **17**, 816–856 (2024).
95. Ali, A. et al. Optimization and characterization of hybrid bio-briquettes produced from the mixture of sawdust, sugarcane bagasse, and paddy straw. *Environ. Sci. Pollut Res.* **31**, 15467–15490 (2024).
96. Zhang, H. et al. Multifunctional carboxymethyl cellulose sodium encapsulated phosphorus-enriched Biochar composites: multistage adsorption of heavy metals and controllable release of soil fertilization. *Chem. Eng. J.* **453**, 139809 (2023).
97. Arun, J., Gopinath, K. P., Vigneshwar, S. S. & Swetha, A. Sustainable and eco-friendly approach for phosphorus recovery from wastewater by hydrothermally carbonized microalgae: study on spent bio-char as fertilizer. *J Water Process. Eng* **38**, 101567 (2020).
98. Sardar, R., Ahmed, S., Shah, A. A. & Yasin, N. A. Selenium nanoparticles reduced cadmium uptake, regulated nutritional homeostasis and antioxidative system in coriandrum sativum grown in cadmium toxic conditions. *Chemosphere* **287**, 132332 (2022).
99. Atif, M. & Perveen, S. Maize grain nutritional quality amelioration with seed-applied thiamine and indole-3-acetic acid under arsenic toxicity. *Environ. Dev. Sustain.* **26**, 101567 (2023).
100. Khan, A. H. A. et al. Ornamental plants for the phytoremediation of heavy metals: present knowledge and future perspectives. *Environ. Res.* **195**, 110780 (2021).
101. Huang, J. et al. Cadmium accumulation characteristics of floricultural plant cosmos bipinnata*. *Chem. Ecol.* **33**, 807–816 (2017).
102. Ighalo, J. O., Omoarukhe, F. O., Ojukwu, V. E., Iwuozor, K. O. & Igwegbe, C. A. Cost of adsorbent Preparation and usage in wastewater treatment: A review. *Clean. Chem. Eng.* **3**, 100042 (2022).
103. Sireesha, S. & Sreedhar, I. Unleashing the potential of Cajanus Cajun Biochar polymer composite for Cu (II) removal: mechanism, modification, and application. *Environ Sci. Pollut Res* https://doi.org/10.1007/s11356-024-33551-z (2024).

104. Hopkins, D. T., MacQuarrie, S. & Hawboldt, K. A. Removal of copper from sulfate solutions using Biochar derived from crab processing by-product. *J. Environ. Manage.* **303**, 114270 (2022).
105. Isaac, R., Siddiqui, S., Aldosari, O. F. & Kashif Uddin, M. Magnetic Biochar derived from juglans regia for the adsorption of Cu2 + and Ni2+: Characterization, modelling, optimization, and cost analysis. *J. Saudi Chem. Soc.* **27**, 101749 (2023).
106. James, A. & Yadav, D. Valorization of coconut waste for facile treatment of contaminated water: A comprehensive review (2010–2021). *Environ. Technol. Innov.* **24**, 102075 (2021).
107. Ranasinghe, S. H., Navaratne, A. N. & Priyantha, N. Enhancement of adsorption characteristics of Cr(III) and Ni(II) by surface modification of jackfruit Peel biosorbent. *J. Environ. Chem. Eng.* **6**, 5670–5682 (2018).
108. Dong, J. et al. Adsorption of copper ion from solution by polyethylenimine modified wheat straw. *Bioresour Technol. Rep.* **6**, 96–102 (2019).
109. Patel, H. Batch and continuous fixed bed adsorption of heavy metals removal using activated charcoal from Neem (Azadirachta indica) leaf powder. *Sci. Rep.* **10**, 1–12 (2020).
110. Yahya, M. D., Abubakar, H., Obayomi, K. S., Iyaka, Y. A. & Suleiman, B. Simultaneous and continuous biosorption of cr and Cu (II) ions from industrial tannery effluent using almond shell in a fixed bed column. *Results Eng.* **6**, 100113 (2020).
111. Fseha, Y. H., Sizirici, B. & Yildiz, I. Phoenix dactylifera (date palm)-Derived Biochar application for the adsorptive removal of multiple inorganics from groundwater for drinking water purposes. *Arab. J. Sci. Eng.* **48**, 12725–12740 (2023).
112. Duan, G., Li, X., Ma, X., Zhong, W. & Wang, S. High-efficiency adsorption removal for Cu(II) and Ni(II) using a novel acylamino dihydroxamic acid chelating resin. *Sci. Total Environ.* **864**, 160984 (2023).
113. Hegazi, H. A. Removal of heavy metals from wastewater using agricultural and industrial wastes as adsorbents. *HBRC J.* **9**, 276–282 (2013).
114. Fouda, A., Hassan, S. E. D., Saied, E. & Hamza, M. F. Photocatalytic degradation of real textile and tannery effluent using biosynthesized magnesium oxide nanoparticles (MgO-NPs), heavy metal adsorption, phytotoxicity, and antimicrobial activity. *J. Environ. Chem. Eng.* **9**, 105346 (2021).
115. Sopanrao, K. S. & Sreedhar, I. Polyvinyl alcohol modified Chitosan composite as a novel and efficient adsorbent for multi-metal removal. *Sep. Purif. Technol.* **340**, 126731 (2024).
116. Fu, C. C., Juang, R. S., Huq, M. M. & Hsieh, C. Te. Enhanced adsorption and photodegradation of phenol in aqueous suspensions of titania/graphene oxide composite catalysts. *J. Taiwan. Inst. Chem. Eng.* **67**, 338–345 (2016).
117. Vukelic, D. et al. Eco-design of a low-cost adsorbent produced from waste Cherry kernels. *J. Clean. Prod.* **174**, 1620–1628 (2018).
118. Sakhiya, A. K., Baghel, P., Anand, A., Vijay, V. K. & Kaushal, P. A comparative study of physical and chemical activation of rice straw derived Biochar to enhance Zn + 2 adsorption. *Bioresour Technol. Rep.* **15**, 100774 (2021).
119. Sakhiya, A. K., Vijay, V. K. & Kaushal, P. Efficacy of rice straw derived Biochar for removal of Pb + 2 and Zn + 2 from aqueous: Adsorption, thermodynamic and cost analysis. *Bioresour Technol. Rep.* **17**, 100920 (2022).

Acknowledgements

The authors thank the staff of Central Analytical Lab for their analytical support and BITS Pilani Hyderabad Campus for facilitating this project.

Author contributions

Sadamanti Sireesha: Investigation, Data curation, Methodology, analysis, characterization of samples and writing original draft.I. Sreedhar*: Supervision; Original Draft-Review and editing; Project mentoring and monitoring.

Declarations

Competing interests

The authors declare no competing interests.

Additional information

Supplementary Information The online version contains supplementary material available at https://doi.org/10.1038/s41598-025-20743-x.

Correspondence and requests for materials should be addressed to I.S.